

## SMELTING SEPARATION BEHAVIORS AND MECHANISMS OF HIGH-ALUMINA RICH-MANGANESE ORE OBTAINED FROM METALLIC REDUCTION AND MAGNETIC SEPARATION

L.-H. Gao, Z.-G. Liu\*, M.-S. Chu\*

\* School of Metallurgy, Northeastern University, Shenyang, China

(Received 17 December 2018; accepted 27 June 2019)

### Abstract

In this paper the smelting separation of high-alumina rich-manganese ore prepared with selective reduction and magnetic separation was proposed to produce the high carbon ferromanganese alloy (HCF<sub>FeMn</sub>). The rational smelting separation parameters for high-alumina rich-manganese ore included the FC/O of 1.1, the smelting temperature of 1550°C, the smelting time of 60 min, and the basicity of 0.7. The smelting separation of high-alumina rich-manganese ore was achieved successfully. The content of Fe, C, Si and other impurities (P, S) were 12.13%, 6.73%, 0.17% and 0.14, 0.008, respectively. Especially, the recovery and the content of Mn reached 80.47% and 76.76%. The obtained high carbon ferromanganese alloy met the higher standard (FeMn78C8) of ferromanganese alloy, especially the content of Si P and S in the HCF<sub>FeMn</sub> alloy was far below the standard value. Based on the SEM-EDS, XRD and thermodynamic calculation, the smelting and separation mechanisms of high-alumina rich-manganese ore was proposed to more effectively explain the effect of smelting parameters on slag/metal separation behaviors during the process of smelting HCF<sub>FeMn</sub> alloys.

**Keywords:** Rich-manganese ore; Smelting separation; High carbon ferromanganese alloy; Thermodynamics

### 1. Introduction

Ferruginous manganese ores are a kind of important manganese resources for manganese extraction. South Africa ranks first in manganese production, with about 4.0 Mt produced and also currently accounts for about 24.1% of the world's identified manganese resources, whereas high-grade manganese ores as an acceptable feed (Mn/Fe mass ratio over 5) for ferromanganese alloys production are a serious scarcity in the global market [1-4]. It has become an indisputable fact that high-quality manganese ore is seriously scarce in the global market. To meet the growing demand, the metallic reduction roasting process -magnetic separation followed by electric furnace process is a brief and suitable way for industrial applications to address high-alumina Fe-Mn ore as a result of selective mining of high-grade manganese ore.

As reported, more than 50% of low-grade manganese ore is a result of selective mining of high grade manganese ore in South Africa. In the previous work, the reduction roasting of low grade manganese ore containing high iron content, followed by

magnetic separation to separate metallic iron and manganese was proposed to produce rich manganese concentrates in nonmagnetic products, and metallic iron in magnetic products [5-8]. Therefore, the Mn and Fe were successfully separated in high-alumina ferruginous manganese ores ( $Al_2O_3 > 7\%$ ,  $SiO_2 < 4\%$ ) by metallic reduction at 1050°C [9]. In addition, few studies have discussed metallic reduction roasting process-magnetic separation followed by electric furnace process to smelt manganese alloy from high-alumina Fe-Mn ores. Nevertheless, it is essential to find a rational understanding for smelting manganese alloy from high-alumina ferruginous manganese ore and propose some suggestions for the smelting process to the utilization of high-alumina Fe-Mn ore.

The high-alumina ferruginous manganese ore from manganese tailing in South Africa with high Al and Fe content will also inevitably obtain high-alumina rich manganese ore (HAMO) containing high Al/Si and Mn/Fe ratio by the above mentioned pre-treatment method. Previous works researched rich manganese ore to smelt HCF<sub>FeMn</sub> alloy, and different Al/Si ratio and Al content in slag compositions were summarized and displayed in Figure 1. Several

\*Corresponding author: liuzg@smm.neu.edu.cn; chms@smm.neu.edu.cn



researchers [10-18] studied and calculated equilibrium phase chemistry in the  $\text{Al}_2\text{O}_3$ - $\text{MgO}$ - $\text{SiO}_2$ - $\text{CaO}$ - $\text{MnO}$  slag system. The slag basicity was optimized by flux addition to obtain the higher manganese recovery and qualified metal with slag containing  $\text{Al}_2\text{O}_3$  content at a range of 7.5 to 16.0 wt %, and an  $\text{Al}_2\text{O}_3/\text{SiO}_2$  weight ratio of 0.2-0.5. In the work of Park et al., [19] the  $\text{Al}_2\text{O}_3$  behaves as an amphoteric oxide with the composition of slags. The influence of alumina on the viscosity decrease can be explained on the basis of a decrease in the degree of polymerization by the increase in the relative fraction of the  $[\text{AlO}_6]$ -octahedral units. The slag transforms from silicates-based to aluminates-based with an increase of Al content and Al/Si ratio [20]. Therefore, the high-alumina rich-manganese ore containing high  $\text{Al}_2\text{O}_3$  content and Al/Si ratio were applied to smelt HCFMn alloy to research the substitution of  $\text{SiO}_2$  with  $\text{Al}_2\text{O}_3$ , and provide an opportunity to explain smelting and separation mechanisms.

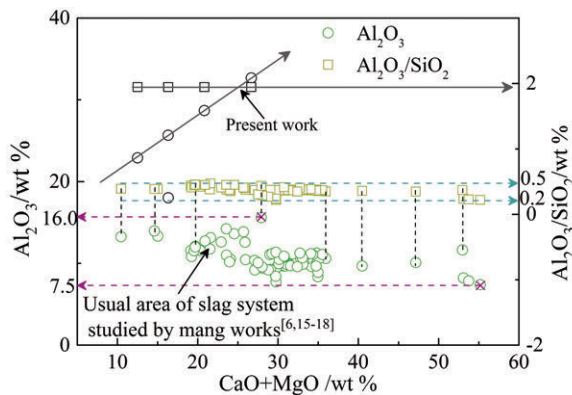


Figure 1. Slag compositions of smelting HCFMn alloy from other workers' studies

## 2. Experiment

### 2.1 Raw Materials

The High-alumina rich-manganese ore was obtained from high-alumina ferruginous manganese ore by metallic reduction roasting and magnetic separation in the author's previous work [9]. The metallic reduction roasting includes reduction temperature 1050°C, time 6 h, particle size 8-13 mm, FC/O 2.5, and magnetic field strength 100 mT. The FC/O is the mole ratio of fixed carbon in coal to reducible oxygen of iron and manganese in low-grade manganese ore or HAMO. The chemical composition and X-ray diffraction (XRD) analysis of HAMO are shown in Table 1 and Figure 2, respectively. It indicated that manganese mainly comprised of MnO and  $\text{MnSiO}_3$ , and the iron compounds mainly existed as metallic Fe and spinelle ( $\text{FeO}\cdot\text{Al}_2\text{O}_3$ ) in HAMO. The Al element in HAMO, which has negative influences on smelting separation of rich manganese

ore, was detected in form of galaxite ( $\text{MnO}\cdot\text{Al}_2\text{O}_3$ ) and hercynite ( $\text{FeO}\cdot\text{Al}_2\text{O}_3$ ). The analytically pure CaO was applied as flux. The activated carbon was used as reduction agent and carburization.

Table 1. Chemical compositions of HAMO /wt %

| TFe  | TMn   | MFe  | MgO  | $\text{Al}_2\text{O}_3$ | CaO  | $\text{SiO}_2$ | S     | P    | Mn/Fe | P/Mn   |
|------|-------|------|------|-------------------------|------|----------------|-------|------|-------|--------|
| 6.15 | 53.48 | 1.91 | 0.64 | 13.21                   | 0.90 | 6.79           | 0.058 | 0.10 | 8.7   | 0.0019 |

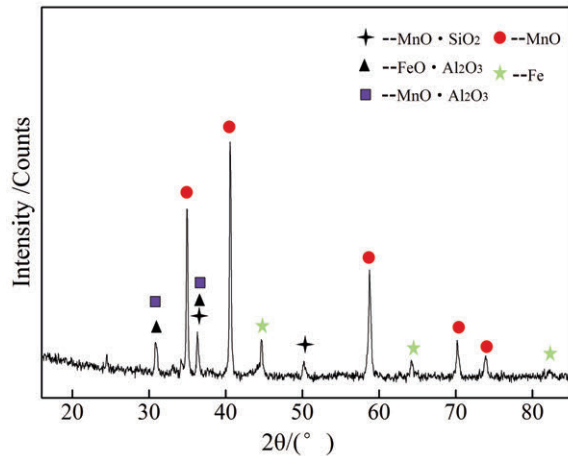


Figure 2. XRD analysis of HAMO

### 2.2 Experimental Procedure

In this paper, the smelting process of HAMO was carried out in a medium frequency induction furnace (XZ-40B) for simulating electric furnace process. The schematic drawing of induction furnace is shown in Figure 3. The experimental apparatus consists mainly of a power control system, a furnace body, a protective gas system, a cooling system, and an induction heating system. The medium frequency induction heating of HAMO with the copper coil are conducted by adjusting the output oscillatory power of control system, and the specified smelting temperature can be achieved within a short time. The copper coil is internally protected by cooling water to prevent superheated melting of copper coil. A

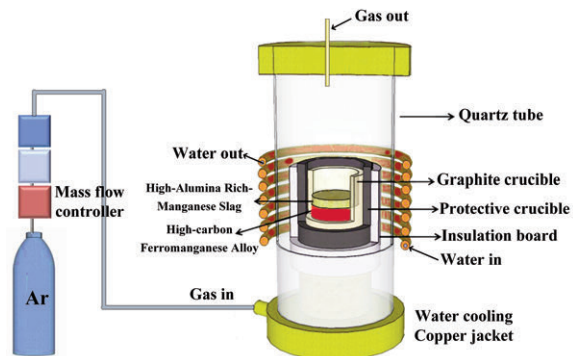


Figure 3. Schematic diagram of induction furnace



calibrated infrared thermometer (DT-8869h) with a measure range of  $-50\sim 2200^{\circ}\text{C}$  and an accuracy of  $0.1^{\circ}\text{C}$  is used for the temperature measurements in the smelting process.

Firstly, the reduced low grade manganese ore was ground by 2-MZ centrifugal grinding machine to 100% passing  $74\ \mu\text{m}$ , followed by magnetic separation using a Davies Magnetic Tube (DTCXG-ZN50) to obtain HAMO in nonmagnetic product and metallic iron in magnetic product. The materials including HAMO powders, activated carbon, and reagent CaO are weighted in a certain proportion. Subsequently, according to the chemical compositions of HAMO, the effect of  $\text{CaO}/(\text{SiO}_2+\text{Al}_2\text{O}_3)$  and FC/O was investigated in the below experiments. The mixtures were loaded in a dense high pure graphite crucible (inner diameter  $\times$  inner height:  $30\ \text{mm}\times 85\ \text{mm}$ , external diameter  $\times$  external height:  $40\ \text{mm}\times 100\ \text{mm}$ ). The crucible was then placed into the effective temperature section of the induction furnace and heated to the designed temperature rapidly to realize separation of HCFeMn alloy and slag. After the smelting separation experiments, the induction furnace was shut down, and the HCFeMn alloy and slag were rapidly cooled down to the room temperature in argon atmosphere.

### 2.3 Experimental Scheme

In the experimental process, the effect of the smelting temperature and time, FC/O and ternary basicity  $\text{CaO}/(\text{SiO}_2+\text{Al}_2\text{O}_3)$  on the separation index was investigated to obtain the rational technological parameters; these parameters ranged  $1450\text{-}1550^{\circ}\text{C}$ ,  $15\text{-}90\ \text{min}$ ,  $0.7\text{-}1.3$  and  $0.4\text{-}0.8$ , respectively. When the CaO fluxes were not added, the smelting basicity of  $\text{CaO}/(\text{SiO}_2+\text{Al}_2\text{O}_3)$  was initially 0.06. The single-factor control variable method was used in this paper, where only a single parameter was changed and the other parameters were kept in the basic conditions. The basic smelting parameters included a smelting temperature of  $1525^{\circ}\text{C}$ , a smelting time of 30 min, a FC/O of 1.1 and a  $\text{CaO}/(\text{SiO}_2+\text{Al}_2\text{O}_3)$  basicity of 0.7. The detailed experimental scheme was listed in Table 2.

**Table 2.** Experimental scheme for the smelting separations of HAMO

| Parameters  | Variation Levels |      |      |      |      |
|---|------------------|------|------|------|------|
|   | 1450             | 1500 | 1525 | 1550 |      |
| Smelting temperature / $^{\circ}\text{C}$                     | 1450             | 1500 | 1525 | 1550 |      |
| Smelting FC/O /-  | 0.7              | 0.9  | 1.1  | 1.3  |      |
| Smelting time /min  | 15               | 30   | 45   | 60   | 90   |
| Smelting $\text{CaO}/(\text{SiO}_2+\text{Al}_2\text{O}_3)$ /- | 0.4              | 0.5  | 0.6  | 0.70 | 0.80 |

After the experiments, the smelting slag and high-carbon ferromanganese alloy (HCFeMn) were obtained and weighed. With the smelting separations of 100 g HAMO, the diameter of obtained alloy was about 30 mm and its height was about 10 mm, as shown in Figure 4. The contents of Mn, Fe, and C elements in high carbon ferromanganese alloy were analyzed by the chemical titrations and ICP-OES analysis to calculate and analyze the recovery and the content of Mn, Fe, and C elements in the HCFeMn alloy. The obtained high-alumina slags were detected by XRD to analyze the phase compositions of smelting slag. The X-ray diffraction of the samples was carried out by using a copper  $\text{K}\alpha$  radiation, with a scanning angle range varied from  $5^{\circ}$  to  $90^{\circ}$  using a scanning speed of  $0.2^{\circ}/\text{s}$ . The microstructure of the smelting sample was observed by scanning electron microscope (SEM) equipped with an energy diffraction spectrum (EDS).

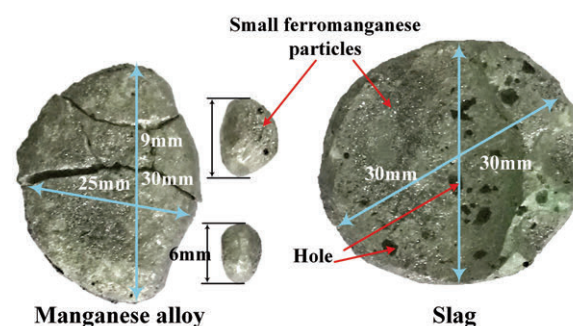


**Figure 4.** Specimens appearance of HCFeMn and high-alumina slags (a) in  $\text{CaO}/(\text{SiO}_2+\text{Al}_2\text{O}_3)$  0.7 and FC/O 0.9 at  $1525^{\circ}\text{C}$  for 30 min

The recovery of valuable elements was calculated according to the following equation:

$$\eta_{Mn} = \frac{m_{Mn} \times \beta_{Mn}}{M_{Mn} \times \gamma_{Mn}} \times 100\% \quad (1)$$

where  $\eta_{Mn}$  is the recovery ratio of manganese in HCFeMn alloy;  $m_{Mn}$  is the mass of HCFeMn alloy;  $M_{Mn}$  is the mass of HAMO;  $\beta_{Mn}$  is the content of manganese in HCFeMn alloy;  $\gamma_{Mn}$  is the content of manganese in HAMO. A similar expression describes how the recovery yield of iron varies with composition in HCFeMn alloy.

## 3. Results and Discussion

### 3.1 Thermodynamic analysis

Figure 5 displays the thermodynamic graph by FACTSAGE 7.0 of reduced manganese oxide and iron oxide in Mn-Fe ore. The mainly reduction reaction relationships are calculated by the following equations (Eq.2-34) in Table 3. Figure 5(a) indicates



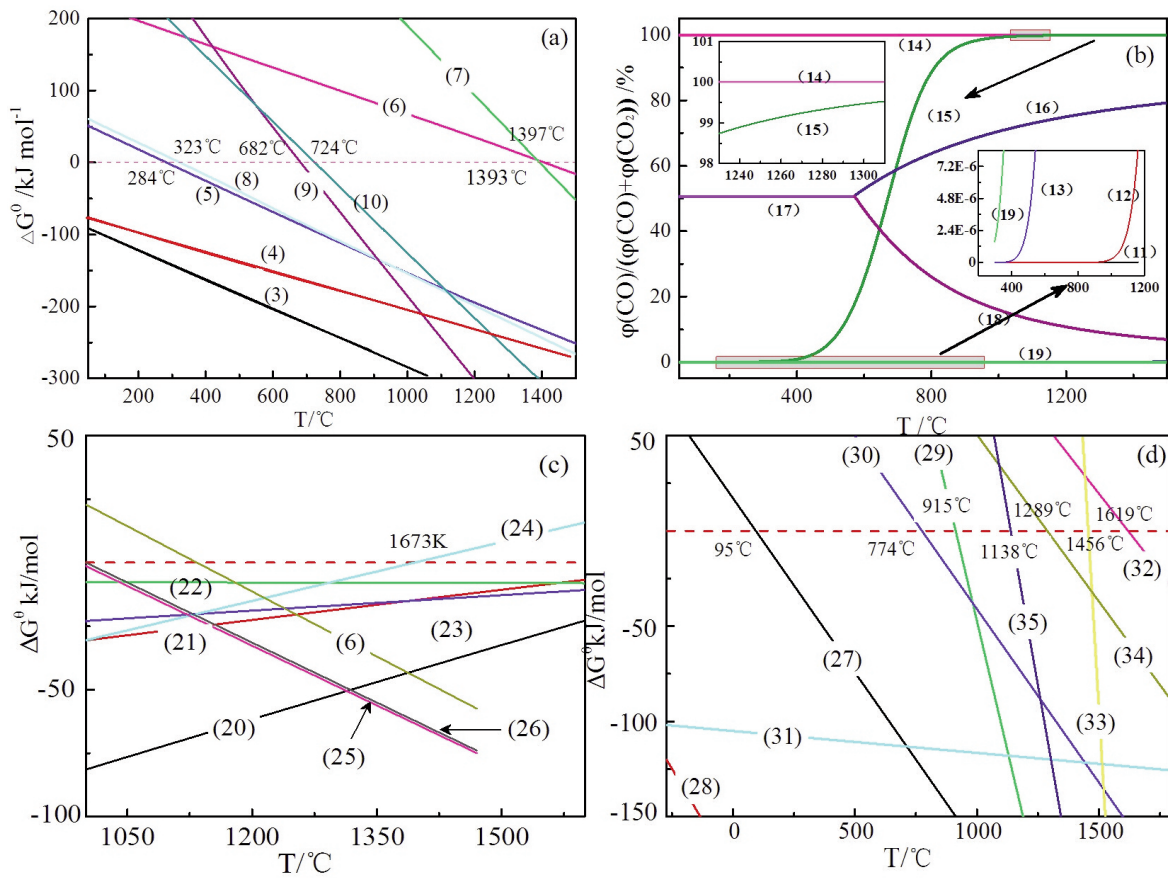


**Figure 5.** Thermodynamics graph of direct reduction (a) and indirect reduction (b) in Mn-Fe ore, the formation of  $Mn_xC_y$  (c) and the decompose of  $Mn_xC_y$  (d)

**Table 3.** The reduction reaction of the Mn-Fe ore based on the following equation

| Reaction equation                     | NO. | Reaction equation                 | NO. | Reaction equation               | NO. |
|---------------------------------------|-----|-----------------------------------|-----|---------------------------------|-----|
| $2MnO_2 + C = Mn_2O_3 + CO$           | 2   | $3Mn_2O_3 + C = 2Mn_3O_4 + CO$    | 3   | $Mn_3O_4 + C = 3MnO + CO$       | 4   |
| $MnO + C = Mn + CO$                   | 5   | $3MnO + C = Mn_3C + 3CO$          | 6   | $3Fe_2O_3 + C = 2Fe_3O_4 + CO$  | 7   |
| $Fe_3O_4 + C = 3FeO + CO$             | 8   | $FeO + C = Fe + CO$               | 9   | $2MnO_2 + CO = Mn_2O_3 + CO_2$  | 10  |
| $3Mn_2O_3 + CO = 2Mn_3O_4 + CO_2$     | 11  | $Mn_3O_4 + CO = 3MnO + CO_2$      | 12  | $MnO + CO = Mn + CO_2$          | 13  |
| $C + CO_2 = 2CO$                      | 14  | $FeO + CO = Fe + CO_2$            | 15  | $Fe_3O_4 + 4CO = 3Fe + 4CO_2$   | 16  |
| $Fe_3O_4 + CO = 3FeO + CO_2$          | 17  | $3Fe_2O_3 + CO = 2Fe_3O_4 + CO_2$ | 18  | $7Mn + 3C = Mn_7C_3$            | 19  |
| $3Mn + C = Mn_3C$                     | 20  | $Mn + 2Mn_7C_3 = 3Mn_5C_2$        | 21  | $5Mn + 2Mn_5C_2 = Mn_{15}C_4$   | 22  |
| $8Mn + 3Mn_5C_2 = Mn_{23}C_6$         | 23  | $7MnO + 10C = Mn_7C_3 + 7CO$      | 24  | $3MnO + 4C = Mn_3C + 3CO$       | 25  |
| $3Mn_7C_3 + 37CO_2 = 7Mn_3O_4 + 46CO$ | 26  | $Mn_3C + 4CO_2 = 3MnO + 5CO$      | 27  | $Mn_7C_3 + 3CO_2 = 7Mn + 6CO$   | 28  |
| $Mn_3C + CO_2 = 3Mn + 2CO$            | 29  | $Mn + CO_2 = MnO + CO$            | 30  | $Mn_7C_3 + 3MnO = 10Mn + 3CO$   | 31  |
| $4Mn_7C_3 + 3Mn_3O_4 = 37Mn + 12CO$   | 32  | $Mn_3C + MnO = 4Mn + CO$          | 33  | $4Mn_3C + Mn_3O_4 = 15Mn + 4CO$ | 34  |

that  $\text{MnO}_2$  and  $\text{Mn}_2\text{O}_3$  should be reduced to  $\text{Mn}_3\text{O}_4$  at lower temperature and then further reduced to  $\text{MnO}$  at above  $284^\circ\text{C}$ . The  $\text{MnO}$  by carbon at atmospheric pressure is reduced to  $\text{Mn}$  and  $\text{Mn}_3\text{C}$  at above  $1393^\circ\text{C}$  and  $1397^\circ\text{C}$ , respectively. The reduction of  $\text{Fe}_2\text{O}_3$  by carbon could be feasible at  $324^\circ\text{C}$ , and the metal  $\text{Fe}$  formed is reduced from  $\text{FeO}$  at  $724^\circ\text{C}$ . As shown in Figure 5(b), the indirect reduction of manganese oxide and iron oxide mainly can be investigated by a thermodynamic graph of manganese and iron oxide. The reduction reaction of  $\text{MnO}_2$ ,  $\text{Mn}_2\text{O}_3$ , and  $\text{Mn}_3\text{O}_4$  is easily converted to  $\text{MnO}$  at a low temperature. Figure 5 (c) illustrates that the initial reaction temperature of  $\text{MnO}$  reduction to  $\text{Mn}_7\text{C}_3$  and  $\text{Mn}_3\text{C}$  is  $1342^\circ\text{C}$  and  $1393^\circ\text{C}$ , respectively. Figure 5(d) shows that  $\text{Mn}_x\text{C}_y$  is easily decomposed by  $\text{CO}_2$ , the  $\text{Mn}_7\text{C}_3$  and  $\text{Mn}_3\text{C}$  can be converted to  $\text{Mn}$  by  $\text{CO}_2$  at  $915^\circ\text{C}$  and  $774^\circ\text{C}$ , respectively.

### 3.2 Effects of $\text{CaO} / (\text{SiO}_2 + \text{Al}_2\text{O}_3)$

The effect of the smelting basicity  $\text{CaO}/(\text{SiO}_2 + \text{Al}_2\text{O}_3)$  on the recovery of Mn and the quality of HCFeMn is given in Figure 6. The smelting basicity  $\text{CaO}/(\text{SiO}_2 + \text{Al}_2\text{O}_3)$  was referred to the molar ratio of  $\text{CaO}$  to  $\text{SiO}_2$  and  $\text{Al}_2\text{O}_3$  in the experimental process. It is obvious that the recovery rate of Mn in HCFeMn increases from 40.80% to 75.92% with an increase of  $\text{CaO}/(\text{SiO}_2 + \text{Al}_2\text{O}_3)$  from 0.4 to 0.7. When the ternary basicity  $\text{CaO}/(\text{SiO}_2 + \text{Al}_2\text{O}_3)$  exceeds 0.7, the recovery of Mn instantly decreases to 70.78%. All the indexes reach the highest at a basicity of 0.7. The recovery of Mn reach 75.92%, and the content of Mn, Fe, and C is 77.04%, 12.50%, and 6.97% in HCFeMn alloy, respectively. When the smelting basicity  $\text{CaO}/(\text{SiO}_2 + \text{Al}_2\text{O}_3)$  in raw ore is 0.06, this slag/metal was not separated successfully. This is mainly due to the sum and polymerization degree of complex viscous units  $[\text{SiO}_4]^{4-}$  tetrahedral and  $[\text{AlO}_4]^{5-}$  tetrahedral in slag are at a high level [21, 22]. High  $\text{Al}_2\text{O}_3$  content in the  $\text{CaO}-\text{SiO}_2-\text{MnO}-\text{Al}_2\text{O}_3$  slag system results in lower absolute amounts of  $\text{SiO}_2$ , which infer that complex silicate structures decrease, and the relative amount of Al-O structures become increasingly dominant. The higher  $\text{Al}_2\text{O}_3$  content increased the slag viscosity due to the polymerization of the aluminate structure. The increasing slag viscosity results in the large viscosity of slag and the poor dynamic conditions for the smelting separation of HAMO which not only impedes the enrichment of Mn in HCFeMn, but also hinders the carbothermal reductions of iron oxides and manganese oxides in the smelting separation process. This is the root cause of the experiment using ternary alkalinity. An increase of  $\text{CaO}/(\text{SiO}_2 + \text{Al}_2\text{O}_3)$  is able to simplify the complex viscous units which leads to the decreased viscosity and improved fluidity in HAMO, mainly because the

$\text{O}^{2-}$  in  $\text{CaO}$  (alkaline oxide) can easily escape from the constraint of  $\text{Ca}^{2+}$  at the high temperature, and it will destroy the network structure of silicate and make the complex  $\text{Si}_x\text{O}_y^z$  [23].

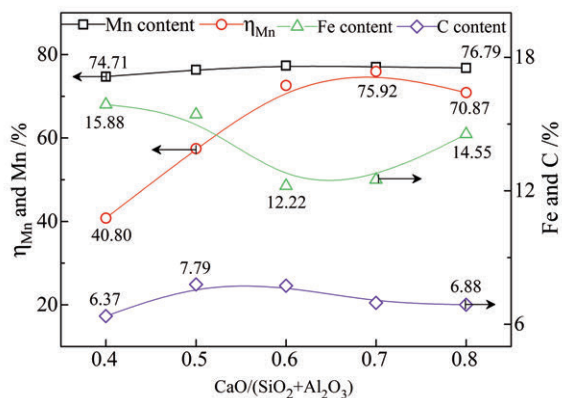


Figure 6. Effect of  $\text{CaO}/(\text{SiO}_2 + \text{Al}_2\text{O}_3)$  on the smelting index

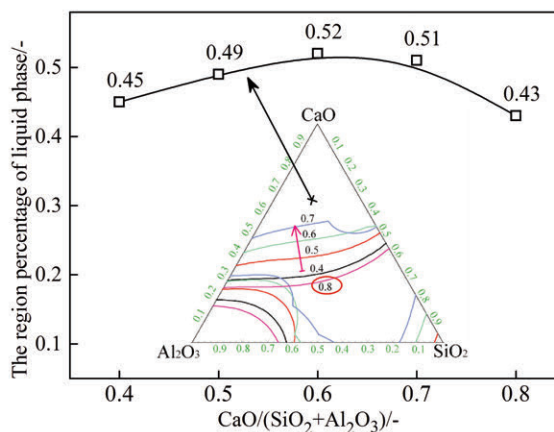


Figure 7. Effect of basicity on the liquid slag region of  $\text{CaO}-\text{SiO}_2-\text{Al}_2\text{O}_3-\text{MgO}-\text{MnO}$

In addition, the Phase Diagram Module in FACTSAGE 7.0 is applied to calculate the phase diagram of the liquid phase region of  $\text{CaO}-\text{SiO}_2-\text{MgO}-\text{Al}_2\text{O}_3-\text{MnO}$  with different  $\text{CaO}/(\text{SiO}_2 + \text{Al}_2\text{O}_3)$  at  $1525^\circ\text{C}$ . The effects of  $\text{CaO}/(\text{SiO}_2 + \text{Al}_2\text{O}_3)$  on the meltability of slag are analyzed to explain the effect of basicity on the efficiency of above various indicators in the smelting process of HAMO. The calculated results are shown in Figure 7. As the basicity increases, the entire area proportion of the full liquid slag enlarges, and the solubility of  $\text{MnO}$  in slag increases simultaneously. When the  $\text{CaO}/(\text{SiO}_2 + \text{Al}_2\text{O}_3)$  reached to 0.8, the area proportion of the liquid slag decreases dramatically. More liquid slag at a certain temperature can promote the complete separation of slag and iron in the smelting separation, which improves the meltability and fluidity of HAMO [24]. Therefore, the effective



separation of HAMO is enhanced with increasing basicity, and the recovery and grade of Mn in pig iron is significantly improved.

To further verify the effects of the  $\text{CaO}/(\text{SiO}_2+\text{Al}_2\text{O}_3)$  on smelting separation of HAMO, the phase composition of separation slag under different basicity is analyzed by XRD in Figure 8. The gehlenite ( $2\text{CaO}\cdot\text{Al}_2\text{O}_3\cdot\text{SiO}_2$ ), and unreduced MnO are detected by XRD in slag, and a little of metal Fe,  $3\text{MgO}\cdot\text{Al}_2\text{O}_3\cdot 3\text{SiO}_2$  and  $\text{MnO}\cdot\text{Al}_2\text{O}_3$  are also simultaneously found. The diffraction peak intensity of MnO is extended with the basicity increasing from 0.4 to 0.7. The effect of slag basicity on the efficiency of smelting separation can be attributed to the activity of MnO in slag. The increased basicity can promote an increase of free MnO which in turn accelerates the reduction of manganese oxide. The basicity of  $\text{CaO}/(\text{SiO}_2+\text{Al}_2\text{O}_3)$  exceeds 0.8, the indexes of smelting have decreases of various degree. In addition, the diffraction peak intensity of gehlenite and MnO at the basicity of 0.8 reaches a higher level, and the area proportion of the liquid slag reaches the lowest value which leads to the increasing liquid temperature of slag. It results in the deteriorated superheat and homogeneity of slag and bring about the increasing viscosity of slag which leads to decreasing the efficiency of the smelting separation [24, 25]. The lower manganese recovery at high basicity can be explained by XRD and thermodynamic calculation in these slags. Therefore, comprehensively considering the experimental results, phase transition, and thermodynamic equilibrium analyses. The rational smelting ternary basicity of  $\text{CaO}/(\text{SiO}_2+\text{Al}_2\text{O}_3)$  in HAMO is approximately 0.7.

### 3.3 Effect of Smelting FC/O

The various indexes in the smelting separation process of HAMO with different smelting FC/O

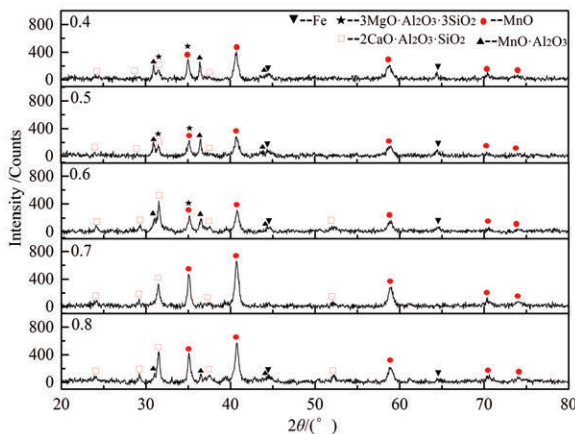


Figure 8. XRD patterns of smelting slag with different ternary basicity of  $\text{CaO}/(\text{SiO}_2+\text{Al}_2\text{O}_3)$

values are described in Figure 9. With an increase of FC/O from 0.7 to 1.3, the recovery rate and content of Mn in HCFeMn increased accordingly from 52.26 to 75.92% and 73.14 to 77.04%, respectively. At a smelting FC/O of 1.1, the recovery and content of Mn reach up to the optimum smelting indexes. Further increasing smelting FC/O to 1.3, the recovery rate, and content of Mn decrease to 67.60% and 76.77%, respectively, and the content of carbon in HCFeMn alloy remains around 7.0%. For the distribution of Fe, its content reaches initially 13.02% at a FC/O of 0.7, and subsequently slowly increases from 12.50% to 13.96% with an increasing of FC/O from 1.1 to 1.3. Therefore, the rational smelting FC/O should be maintained at 1.1 for smelting separation process of HCFeMn alloy.

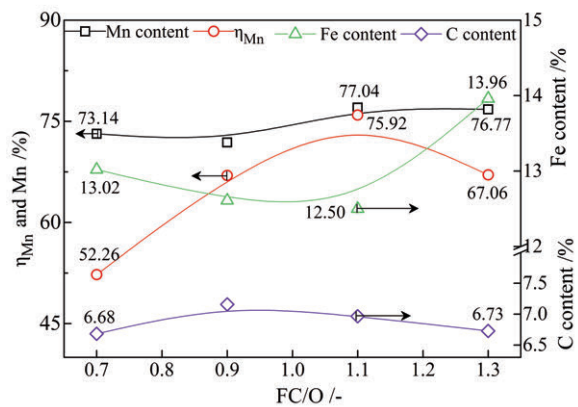
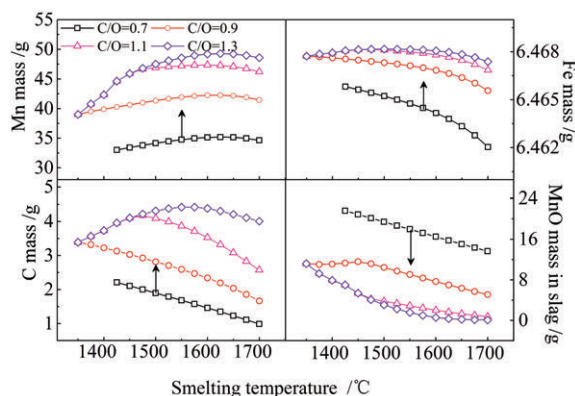


Figure 9. Effect of smelting FC/O on the smelting separation of HAMO

To further investigate the effect of smelting FC/O in the smelting separation of HAMO, the Equilib Module in Factsage 7.0 packages is applied to assess the thermodynamic equilibrium. 100 g of the mixed samples were analyzed at the temperature range of 1350°C - 1700°C. The relative amount variation of the main products is shown in Figure 10. With increasing the smelting FC/O from 0.7 to 1.1, the generation mass of liquid Mn (l) is significantly improved, meanwhile the mass of nonmetal C in the metal also declines. In addition, the mass of MnO phases in the slag gradually decreases which proves that carbothermal reductions of MnO are significantly improved. Further, the smelting FC/O increasing from 1.1 to 1.3, the generating amount of Mn, Fe and C in the metal slowly grows at the smelting temperature of 1600°C. For the mass of Fe in metal, the generated amount of Fe (l) in metal does not result in significant fluctuations. It is mainly due to the reduction of FeO in the main iron reduction stage which can occur by dissolved carbon as the dominant reaction in the product metal at the initial stage. And FeO does not easily polymerize with the flux and is easily reduced

by carbon in the initial stage. Therefore, comprehensively considering the experimental results and thermodynamic equilibrium analyses, the rational smelting FC/O of HAMO is approximately 1.1.



**Figure 10.** Thermodynamic equilibrium analyses using FACTSAGE 7.0 with different smelting FC/O values, the Mn, Fe and C mass in metal, and MnO mass in slag

### 3.4 Effect of Smelting Time

The variation of smelting separation index at different smelting time of HAMO is shown in Figure 11; it indicates that the recovery rate and the content of Mn in HCFeMn alloy at the initial stage increases from 39.42% to 75.92, and from 72.40% to 77.04%, with an increase of the smelting time from 15 min to 60 min. However, the content of carbon and iron in HCFeMn alloy decreases from 8.27% to 6.97%, and from 16.75% to 12.70%, respectively. At the smelting time of 60 min, the recovery rate and the content of manganese reach 75.92% and 77.04%, respectively. Further, an increase of the smelting time declines tardily the recovery rate and the content of manganese in HCFeMn alloy.

The XRD analysis of reduced HAMO at different smelting time is shown in Figure 12. When smelting

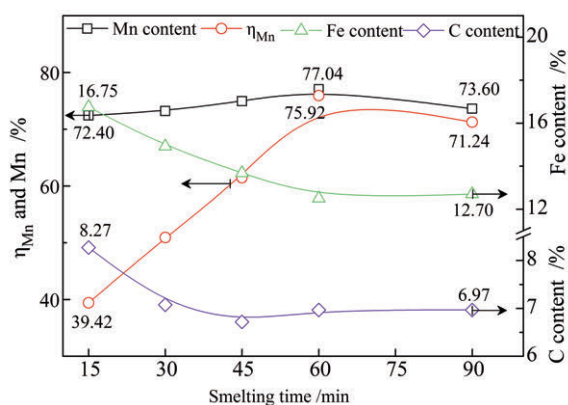


**Figure 11.** Effect of smelting time on the smelting index

time is under 60 min, the diffraction peaks of MnO get weaker gradually, which demonstrates that MnO in HAMO is reduced by carbon with an increase of the smelting time. The diffraction peaks of gehlenite as the basic phases maintain stabilization. However, when the smelting time reaches 90 min, the diffraction peaks of MnO remarkably decrease, while the peaks value of gehlenite clearly increases due to the complete reduction of manganese oxidation in HAMO. It can explain that the content of iron and carbon in the alloy gradually declines with an increase of smelting time. When the time is longer than 60 min, both the recovery rate and the content of Mn decrease. This is primarily due to manganese vaporization losses in the smelting process. At the initial smelting reduction stage, the Fe metal serves as a reservoir for Mn formed from MnO reduction and thus limits manganese vaporization losses; the formation of this Fe-Mn alloy results in the lowered activity of manganese, as compared to pure manganese formation resulting in favorable thermodynamics to drive the MnO reduction reaction [26]. At the later stage, little or no metallic iron and FeO in the slag, the produced Mn by carbothermic reduction is rapidly evaporated due to high vapor pressure of Mn at high temperature [27].

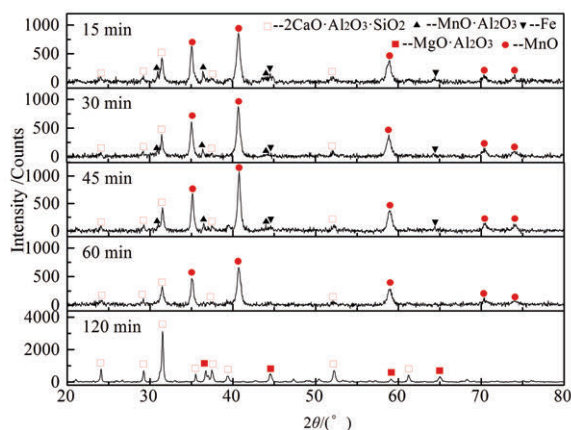


**Figure 12.** XRD patterns of smelting slag with different smelting time

To further confirm the effects of smelting time of the smelting separation of HAMO, various compositions of slag after the smelting separation were analyzed by SEM and EDS. The results are presented in Figure 13. There are three main phases in the samples. The white is Mn-Fe particles; the light gray (Point C) is the slag containing mainly MnO, and the dark gray (Point B) is the slag containing a lot of gehlenite and a little spinel, not only by EDS analysis but also by XRD analysis. Furthermore, it is obvious that the Fe-Mn alloy and the unreduced phase MnO are closely connected and not effectively separated with each other at the smelting time of 15 min (Figure

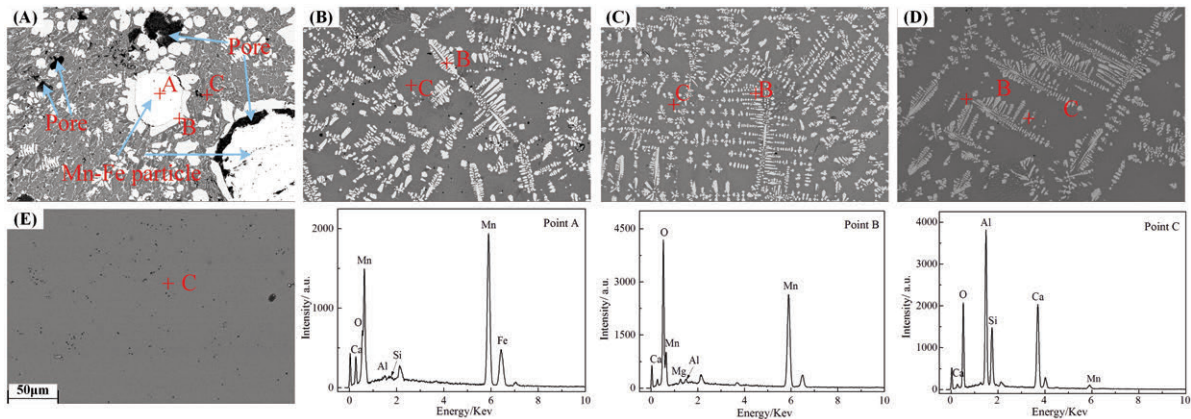


**Figure 13.** SEM-EDS analyses of the smelting slag with different smelting time: (A) 15 min, (B) 30 min, (C) 45 min, (D) 60 min and (E) 90 min

13(A)). The Fe-Mn particles are carburized after their initial formation [26]. With increasing the smelting time, the phase of MnO in the slag gradually decreases. Figure 13 (A) shows that the slag droplet forms and moves during the reduction of the smelting separation. Numerous pores formation is caused by CO gas bubble formation ore or aggregation and growth of metal particle in the slag. The comparison of the SEM analysis, only a small amount of MnO phase in the Mn-Fe slag are found in Figure 13(E). This explains why the carbothermic process of MnO in the slag is basically completed. Therefore, if the smelting time is short (< 45 min) or too long (> 60 min), the short smelting time is not enough for the deep reduction and carburization. But, the long smelting time will cause the increasing manganese vaporization losses in the smelting process [27, 28]. Therefore, comprehensively considering the experimental results, XRD and SEM-EDS analyses, rational smelting time of HAMO is approximately 60 min.

### 3.5 Effects of Smelting Temperature

The effect of smelting temperature on the Mn recovery and the content is shown in Figure 14. The recovery and the content of Mn increase from 27.18 to 80.47%, and from 67.87 to 76.76% with the smelting temperature raising from 1475 to 1550°C, respectively. The content of Fe and C slightly decreases from 16.55 to 12.13%, and from 7.04 to 6.73% at an increase of the smelting temperature. Especially, at the smelting temperature of 1550°C, the recovery and the content of Mn reach 80.47% and 76.76%.

The XRD patterns of smelting separation slag are described as Figure 16. The key precipitated phases of slag are gehlenite and MnO. Furthermore, the minor manganese spinel and metal iron can also be found. With the temperature increasing from 1475 to

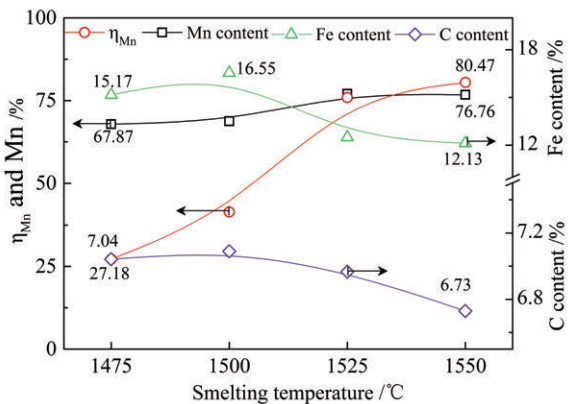


**Figure 14.** Effect of smelting temperature on the smelting index

1550°C, the gehlenite and MnO phase in the precipitated phase obviously changes. And the diffraction peaks of complex gehlenite gradually increase, while the diffraction peaks of MnO decrease. It proves the effect of the smelting temperature on the carbothermic reaction of the free MnO. Especially, at 1550°C, the diffraction peaks of gehlenite are clearly higher than other temperatures, only a small amount of MnO phase is detected by XRD. According to the thermodynamic phase diagram analysis (Figure 10), the content of Mn Fe and C in HCFEMn alloy maintains basically constant which proves that the smelting temperature has less influence on the content of element in HCFEMn alloy when the temperature exceeds 1550°C. The morphology of the separation between alloy and slag with different smelting temperatures is shown in Figure 15. The morphology of HCFEMn alloy has obvious changes with different smelting temperatures. Obviously, a large number of Fe-Mn particles retained in the slag at the smelting temperature of 1475°C, and the aggregation and growth of Fe-Mn particle in the slag appears, but the smelting separation is not achieved successfully due to the big viscosity and bad

fluidity of the slag at lower temperatures. Accordingly, it is necessary to further study the separation mechanism of HAMO, which can be seen in the following work. In Figures 17 (A), one can find Fe-Mn enriched phase droplets dispersed in the slag phase at low smelting temperature, which proves that low temperature has a significant impact on the separation of slag and Fe-Mn alloy. The higher the smelting temperature, the better the smelting separation of slag in Figure 14 and Figure 17 (C and D).

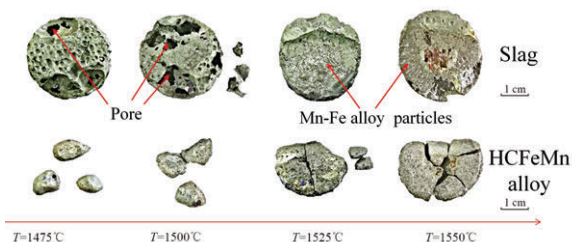


Figure 15. Morphologies of the separation iron and slag with different smelting temperature

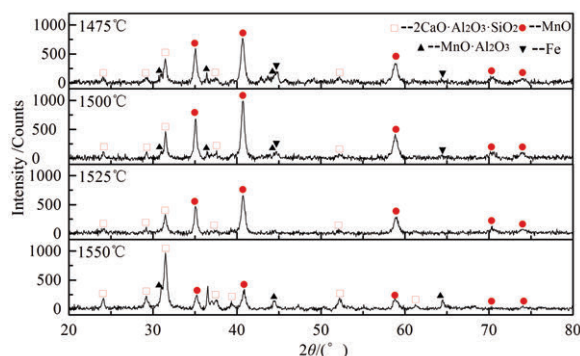


Figure 16. XRD patterns of smelting slag with different smelting temperature

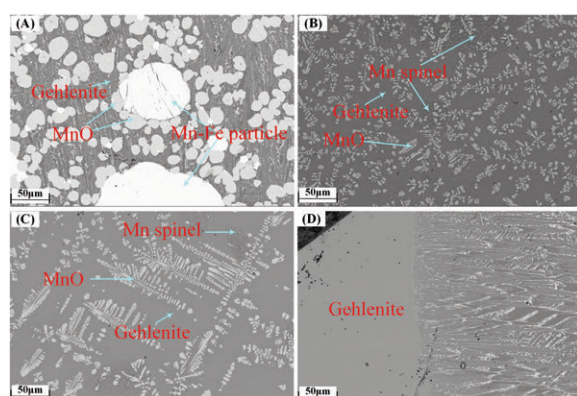


Figure 17. SEM-EDS analysis of the smelting slag with different smelting temperature: (A) 1475°C; (B) 1500°C; (C) 1525°C; (D) 1550°C

### 3.6 Microstructure of ferromanganese and smelting slag

Based on the effect of smelting the parameters on the recovery and grade of the valuable elements of HAMO in the smelting separation process, the rational smelting parameters of HAMO includes the  $\text{CaO}/(\text{SiO}_2+\text{Al}_2\text{O}_3)$  of 0.7, the  $\text{FC}/\text{O}$  of 1.1, the smelting temperature of 1550°C and the smelting time of above 60 min. The test under the related optimal smelting separations of HAMO (time: 60 min) is carried out. The content of Fe, C, Si and other impurities (P, S) is 12.13%, 6.73%, 0.17%, and 0.14, 0.008, respectively. The recovery and the content of Mn reach around 80.47% and 76.76%, respectively. In addition, the volatilization of Mn is about 8.75% in the process of smelting a ferromanganese alloy. It was listed in Table 4. During the steelmaking process, the HCFeMn alloy is added as a desulfurizer, a deoxidizer, or an alloy additive. The HCFeMn alloy is classified by their Mn, Si, C contents and other impurities. Compared with the national standard of HCFeMn alloy in China, the HCFeMn alloy meets the higher Chinese Standard (GB/T3795-2014) of ferromanganese alloy (FeMn78C8).

Table 4. Chemical composition of the ferromanganese alloy (wt %)

| Elements     | Mn        | C    | Si   |     | P    |      | S     |
|--------------|-----------|------|------|-----|------|------|-------|
|              |           |      | I    | II  | I    | II   |       |
| FeMn78C8.0   | 75.0~82.0 | 8.0  | 1.5  | 2.5 | 0.20 | 0.33 | 0.03  |
| FeMn74C7.5   | 70.0~77.0 | 7.5  | 2.0  | 3.0 | 0.25 | 0.38 | 0.03  |
| FeMn68C7.0   | 65.0~72.0 | 7.0  | 2.5  | 4.5 | 0.25 | 0.40 | 0.03  |
| HCFeMn alloy | 76.76     | 6.73 | 0.17 |     | 0.14 |      | 0.008 |

The SEM-EDS analyses of metal and slag after the optimal smelting separation of HAMO are shown in Figure 18 and 19. It can be seen that the metal and slag are achieved successfully, and the Mn-rich with Fe and C is extensively distributed in the metal. In addition, the gehlenite phase and the MnO phase in the slag are clearly separated from each other. The Fe-Mn particles are not detected in the slag. The distribution of elements in the metal is clearly shown in Figure 19. It is revealed that most elements of Mn, Fe, and C are evenly distributed in the HCFeMn alloy. It is difficult to find the aggregation of sulphur and phosphorus impurity in the metal, but the distribution of impurity P element occurs aggregation phenomenon in a certain area of slag.



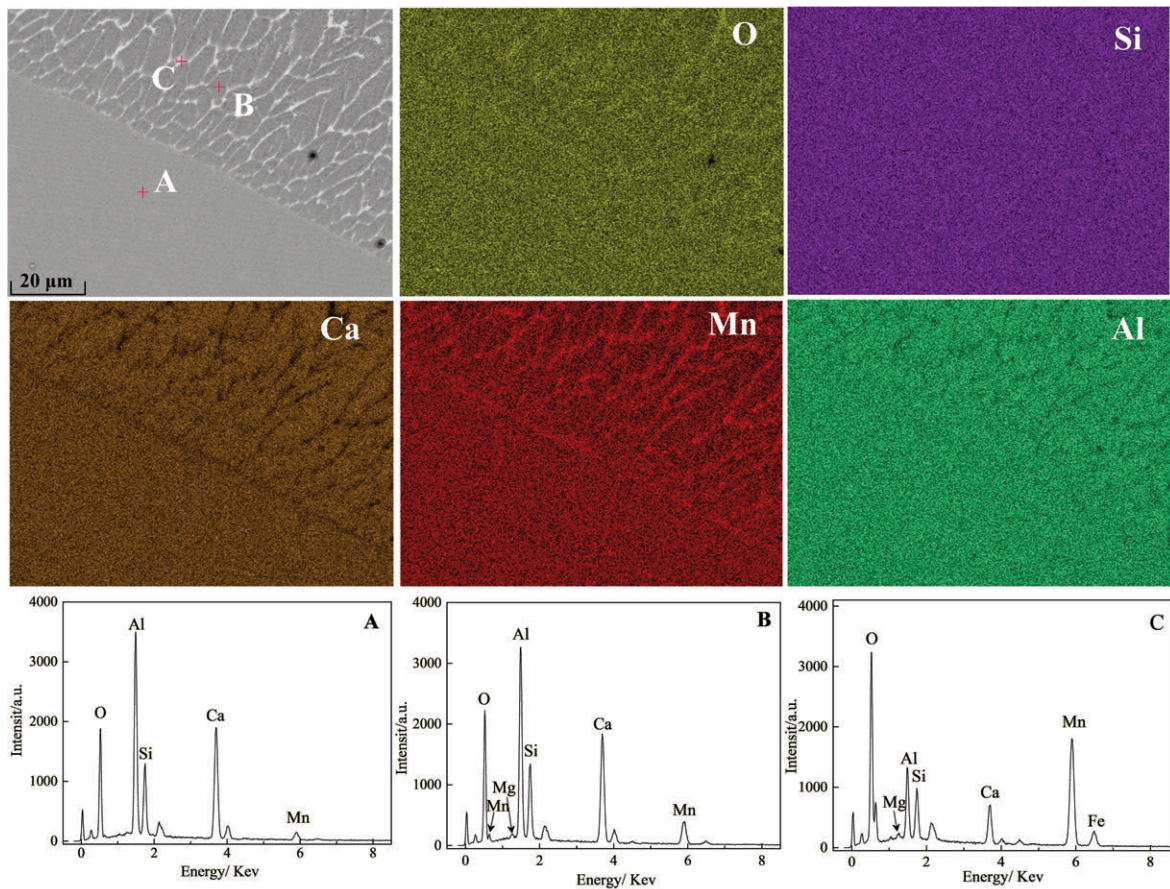


Figure 18. SEM-EDS analyses of smelting slag

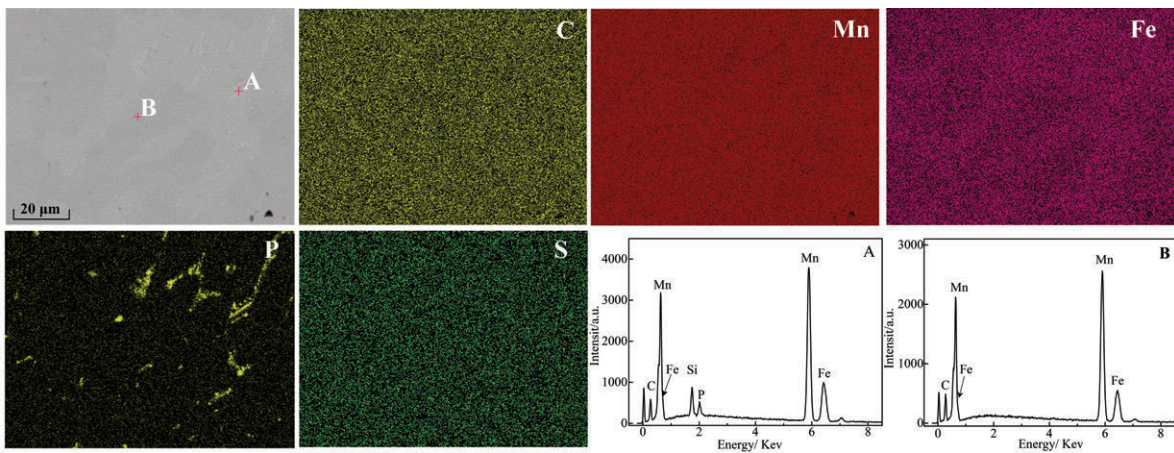


Figure 19. SEM-EDS analyses of HCFeMn alloy

#### 4. Conclusion

In this paper, the smelting and separation mechanisms of high-alumina rich-manganese ore were proposed to produce the excellent high carbon

ferromanganese alloy (HCFeMn). The main conclusions can be summarized as follows:

The optimized smelting separation parameters for high-alumina rich-manganese ore includes a smelting temperature of 1550°C, a smelting time of 60 min, a CaO/(SiO<sub>2</sub>+Al<sub>2</sub>O<sub>3</sub>) of 0.7, and a FC/O of 1.1. The

smelting separation of high-alumina rich-manganese ore was achieved successfully. The content of Fe, C, Si and other impurities (P, S) is 12.13%, 6.73%, 0.17% and 0.14, 0.008, respectively. Especially, based on the abovementioned parameters, the recovery and content of Mn reach around 80.47% and 76.76%. The obtained high carbon ferromanganese alloy meets the higher standard (FeMn75C7.5) of ferromanganese alloy.

Based on the SEM-EDS, XRD and thermodynamic calculation, the smelting and the separation mechanisms of high-alumina rich-manganese ore were proposed to more effectively explain the effect of the smelting parameters on slag/metal separation behaviors during the process of smelting HCFeMn alloys. It can be seen that the metal and slag are achieved successfully. The Mn-rich with Fe and C is extensively distributed in the metal. The main gehlenite phase and the MnO phase in the slag are clearly separated from each other. It is difficult to find the aggregation of sulphur and phosphorus impurity in the metal, and the distribution of impurity P partly occurs aggregation phenomenon in a certain area of slag.

#### Acknowledgements

*The authors wish to express their thanks to the National Natural Science Foundation of China (51704061) and Fundamental Research Funds of the Central Universities of China (N162503003) for financial support.*

#### References

- [1] T. Coetsee, Miner. Process. Extr. Metall. Rev., 39 (5) (2018) 351-358.
- [2] G. Li, Z. Peng, L. Qin, Y. Zhang, T. Jiang, J. Min. Metall. Sect. B-Metall., 53 (2) B (2017) 115-122.
- [3] Y.B. Zhang, B.B. Liu, Z.X. You, Z.J. Su, W. Luo, G. Li, T. Jiang, Miner. Process. Extr. Metall. Rev., 37 (5) (2016), 333-341.
- [4] S.F. Xiong, X. Li, P.L. Liu, S.H. Hao, F. Hao, Z.L. Yin, J.X. Liu, Miner. Eng., 125 (15) (2018), 126-132.
- [5] E.C. Vanderstaay, D.R. Swinbourne, M.A. Monteiro, Miner. Process. Extr. Metall. Rev., 113 (2004) 38-44.
- [6] Y.B. Zhang, M.H. Du, B.B. Liu, Z.J. Su, G.H. Li, T. Jiang, Sep. Sci. Technol., 52 (2017) 1321-1332.
- [7] Y.B. Gao, M. Olivas-Martinez, H.Y. Sohn, G.K. Hang, W.K. Chan, Metall. Mater. Trans. B, 43 (2012) 1465-1475.
- [8] V. Singh, T.K. Ghosh, Y. Ramamurthy, V. Tathavadkar, Int. J. Miner. Process, 99 (2011) 84-86.
- [9] L.H. Gao, Z.G. Liu, M.S. Chu, R. Wang, Z.H. Wang, C. Feng, Sep. Sci. Technol., 54 (2019) 195-206.
- [10] T. Coetsee, C. Reinke, J. Nell, P. C. Pistorius, Metall. Mater. Trans. B, 46 (2015) 2540-2552.
- [11] J. Safariana, L. Kolbeinsen, Metall. Mater. Trans. B, 46 (2015) 125-134.
- [12] J. Safarian, L. Kolbeinsen, M. Tangstad, G. Tranell, Metall. Mater. Trans. B, 40 (2009) 935-939.
- [13] T. Coetsee, J. Nell, P. C. Metall. Mater. Trans. B, 48 (2017) 1463-1485.
- [14] H. Jung, Y. B. Kang, S. A. Decterov, A. D. Pelton, Metall. Mater. Trans. B, 35 (2004) 264-268.
- [15] J. Safarian, G. Tranell, L. Kolbeinsen, M. Tangstad, S. Gaal, J. Kaczorowski, Metall. Mater. Trans. B, 39 (2008) 704-705.
- [16] L. Jin, H. Wang, Z. Xu, F. Wang, J. Univ. Sci. Technol. B, 29 (6) (2007) 574-577.
- [17] Y. Zhao, J. Zhang, China's manganese industry, 14(4) (1996) 47-50. (In Chinese)
- [18] An, X. Zheng, H. China's manganese industry, 19(3) (2001) 26-29. (In Chinese)
- [19] J.H. Park, H. Kim, D.J. Min, Metall. Mater. Trans. B, 39 (2008) 150-153.
- [20] Z.M. Yan, X.W. Lv, D. liang, J. Zhang, C. G. Bai, Metall. Mater. Trans. B, 48 (2017) 1092-1099.
- [21] Z.W. Zhang, S.C. Chen, X. Wu, Z.T. Guo, H.J. Yang, G. Chen, J. Iron. Steel. Res. Int., 41 (4) (2013) 4-6.
- [22] C. Feng, M.S. Chu, J. Tang, Z.G. Liu, Int. J. Miner Metall. Mater., 25 (2018) 609-622.
- [23] I. Sohn, D.J. Min, Steel. Res. Int., 83 (7) (2012) 621-630.
- [24] J. Tang, M.S. Chu, C. Feng, Y. Tang, Z.G. Liu, ISIJ Int., 56 (2) (2016) 210-213.
- [25] L. Zhang, L.N. Zhang, M.Y. Wang, G.Q. Li, Z.T. Sui, Miner. Eng., 20 (7) (2007) 684-688.
- [26] J. Safarian, L. Kolbeinsen, ISIJ Int., 20 (7) (2007) 684-688.
- [27] S.W. Joo, S.H. Hong, G.H. Lee, B.D. You, Met. Mater. Int., 19 (3) (2013) 585-590.
- [28] A. Blagus, J.R. Dankwah, V. Sahajwalla, ISIJ Int., 20 (7) (2007) 684-688.



## PONAŠANJE I MEHANIZMI RAZLAGANJA TOPLJENJEM RUDE MANGANA BOGATE GLINICOM DOBIJENE POSTUPKOM REDUKCIJE I MAGNETNE SEPARACIJE

L.-H. Gao, Z.-G. Liu\*, M.-S. Chu\*

\* Metalurški fakultet, Severnoistočni univerzitet, Šenjang, Kina

### Apstrakt

Da bi se proizvela legura fero-mangana sa visokim udelom ugljenika (HCFeMn) u ovom radu je predložen postupak separacije topljenjem rude mangana bogate glinicom pripremljene selektivnom redukcijom i magnetnom separacijom. Racionalni parametri separacije topljenjem aluminatne rude bogate magnezijumom uključuju FC/O od 1.1, temperaturu topljenja od 1550°C, vreme topljenja od 60 minuta, i bazicitet od 0.7. Separacija topljenjem rude mangana bogate glinicom uspešno je izvedena. Sadržaj Fe, C, Si i drugih primesa (P, S) su 12.13%, 6.73%, 0.17% i 0.14, 0.008 pojedinačno. Dobijanje i sadržaj Mn dostižu oko 80.47% i 76.76%. Dobijena fero-mangan legura sa visokim udelom ugljenika zadovoljava više standarde (FeMn78C8) fero-mangan legure, i što je posebno, sadržaj Si P i S u HCFeMn leguri je daleko ispod standardnih vrednosti. Na osnovu SEM-EDS, XRD i termodinamičkih proračuna, mehanizmi topljenja i separacije rude mangana bogate glinicom su predloženi da bi se efikasnije objasnio efekat parametara topljenja na separaciju šljake/metala tokom procesa topljenja HCFeMn legura.

**Ključne reči:** Ruda bogata manganom; Separacija topljenjem; Fero-mangan legura sa visokim udelom ugljenika; Termodinamika.

